

Article

SS 433: Flares and L_2 Overflow Spirals

Michael Bowler

Department of Physics, University of Oxford, Keble Road, Oxford OX1 3RH, UK;
michael.bowler@physics.ox.ac.uk

Abstract: Flaring in the SS 433 microquasar is dominated by outbursts from material at distances from the centre of mass of the binary system comparable to the separation of the two components. This note completes a demonstration that ejected plasma leaves the system in the region of the L_2 point, there overflowing the outer Roche lobe and giving rise to a spiral structure as it leaves the system as part of the local environment. It also provides a new measure of the mass ratio of the binary.

Keywords: X-rays; binaries; ULX; stars; SS 433; galaxies; stellar content; microquasar

1. Introduction

The Galactic microquasar SS 433 is best known for its precessing jets and for being, in all probability, the only ULX source in the Galaxy. The source of the jets lies in accretion of material transferred from an overflowing Companion to a compact object, a black hole. The components of this binary system have, respectively, masses of (approximately) 25 and $15 M_\odot$ [1]. The orbital speed of the compact object is $\sim 175 \text{ km s}^{-1}$ (see [2]). The precessing jets, initially defining a cone, are collimated into a cylindrical conformation about 40 pc from launch. The collimated jets punch through the expanding supernova remnant to produce extrusions in the nebula W50, which envelopes the central engine. In the process of collimation, it seems that shocks are responsible for generating TeV gamma radiation [3]. The collimation is the result of ambient pressure in the SNR cavity [4], in turn dependent on the interstellar environment; collimation is expected to take place 35 pc downstream [5], just where the origin of the TeV gammas is located [3]. The environment of SS 433 is not only of interest on this scale; the more that is understood about the environment of this unique object, the better. Here, we are not concerned with the recent TeV gamma observations, but with the phenomenon of flaring, which occurs on the very different scale of the binary structure, $\sim 1 \text{ mpc}$.

These flares are observed primarily as intermittent outbursts in intensity. As such, a sustained period of observation is required for their detection. Continuous monitoring at radio wavelengths has been straightforward, but data at shorter wavelength become progressively harder to acquire. A remarkable sequence of observations of flaring in Balmer $H\alpha$ reveals not only intensity changes but also the changes in the shape of the spectral line as high velocity material appears. The original daily $H\alpha$ spectra may be seen in [6], an analysis of these flare data, accompanied by radio at 2.15 GHz, in [7]. The flare onset is rapid and manifested in a broad and complex spectral structure, decomposed into typically five components after the flare initiates. The wind from the accretion disk doubles in speed, and the speed of the jets increases. Red and blue shifted extreme components appear simultaneously, with Doppler shifts $\sim 500 \text{ km s}^{-1}$. The general appearance of the extreme components is what might be expected from a ring rotating with this speed and looked at almost edge on. Those data were originally interpreted as radiation from the accretion disk [7,8], and this interpretation proved to be completely wrong [9].

The origins of TeV photons and X-rays have been located some 35 pc away from the central engine and sources of radio emission on a similar scale. The origin of flare $H\alpha$ on the outskirts of the binary, $\sim 1 \text{ mpc}$ out, has been established only recently [9], reviewed



Citation: Bowler, M. SS 433: Flares and L_2 Overflow Spirals. *Galaxies* **2024**, *12*, 40. <https://doi.org/10.3390/galaxies12040040>

Received: 16 June 2024

Revised: 16 July 2024

Accepted: 16 July 2024

Published: 18 July 2024



Copyright: © 2024 by the author. Licensee MDPI, Basel, Switzerland. This article is an open access article distributed under the terms and conditions of the Creative Commons Attribution (CC BY) license (<https://creativecommons.org/licenses/by/4.0/>).

briefly in Section 3. This paper is concerned with the spatial structure of the outflow on this miniscule scale.

2. The H α Data

The most relevant representation of these deceptive data is provided in Figure 1, originally shown in [8] (and again in [9]). The red and blue flare components were fitted to Gaussian distributions and the Doppler shifts of the mid points plotted, day by day, as a function of the phase of the binary system. The red and the blue swing together from the red (at phase 0.75) to the blue (at 1.25). Separated by $\sim 1000 \text{ km s}^{-1}$, they each exhibit a change in velocity of $\sim 350 \text{ km s}^{-1}$. This is just twice the orbital velocity of the compact object itself and is the most deceptive feature of these data; it almost demands interpretation as radiation from an accretion disk about the compact object. There are some minor features in addition. The two trajectories draw apart with time (suggesting that the supposed ring or disk rotates faster as time goes on). It also appears that the maximum red and blue shifts of the trajectories move to later phases. The curves in Figure 1 represent a very simple model embodying these features, a rotating ring (speeding up with time) in orbit about the compact object, augmented by an infalling stream on its way to join the accretion disk and hence streaming in its direction. Such a stream would augment the red component from the receding edge of the disk between phases of 0.75 and 0.25. Similarly, such a stream would augment the blue component from the rotating disk between 0.25 and 0.75 (for details, see Equations (1) and (2) in [8]). This crude model captured the principal features well, in particular, the difference of 350 km s^{-1} (between the extremes of variation with orbital phase).

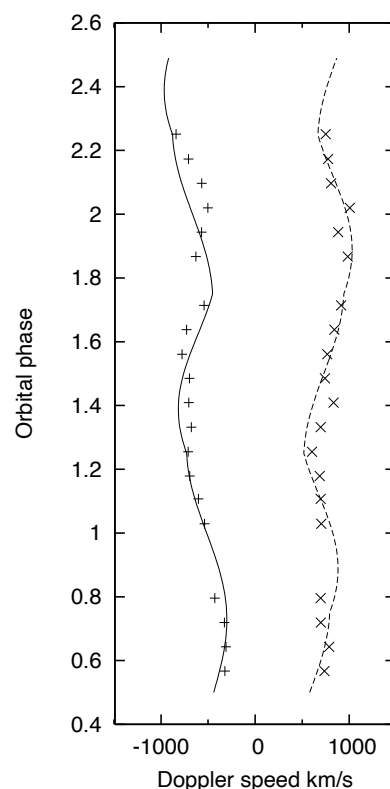


Figure 1. The Doppler shifts of the blue and red flare components as orbital phase advances (from [8,9]). The superimposed curves assumed the source to be the accretion disk, because of the distinct memory of orbital phase. They could equally well describe L_2 expulsion of Roche lobe overflow (see text).

3. The Red and Blue Flares Cannot Be Glimpses of the Accretion Disk

What could be wrong is that the radius of the accretion disk, given a rotational velocity $\sim 500 \text{ km s}^{-1}$, would have to be visible deep inside the photosphere surrounding the compact object. Then, in 2017, interferometric measurements using the GRAVITY instrument [10] sampled a $\text{Br}\gamma$ signal in (angular) position as well as red shift, finding speeds $\sim 500 \text{ km s}^{-1}$ at radii from the system centre of mass $\gtrsim A$ (A being the separation of the two components of the binary). These observations were interpreted in [10] in terms of a circumbinary disk, both rotating and expanding radially. This stimulated me to investigate whether it would be possible to distinguish $\text{H}\alpha$ spectra from an accretion disk, as opposed to from material in the outer regions of the system. To my considerable surprise, I obtained an unambiguous result [9]. Those flare spectra did not experience any eclipse by the Companion and so could not be a series of views of the accretion disk. This raised an important question: if their source is not attached to the compact object, then how could it be that the trajectories exhibited a Doppler shift of $\sim 350 \text{ km s}^{-1}$ between extremes, separated by half the orbital period of the binary?

If the intermittent flares are the result of the (comparatively) normal Companion overflowing the Roche lobes, the overflow is likely to favour the region of the L_2 point. This point rotates with the same angular velocity as the compact object—the centre of mass of the binary, the compact object and the L_2 point lie on a straight line—and so the effluent is likely to retain some memory; on an escape orbit, it drifts outward and slows down. If ejecta leave the L_2 point, at perhaps 500 km s^{-1} towards us, the ejecta from half a period earlier are now further out and now slower (with a corresponding red shift). After another half period, we observe the full red shift (and the blue is less blue). Thus, the red trajectory in Figure 1 (and, with it, the blue) oscillates with time (that is, orbital phase), having the period of rotation of the system, 13.8 days. The difference in recessional speeds is responsible for the perceived difference in the Doppler shift between phase 0.75 and on to 0.25. This is as far as the analysis went in [9], as it was primarily concerned with the evidence that the flare spectra were not visions of the accretion disk, but formed in the wider environment. This paper takes up the investigation at that point.

It must be a coincidence that this speed difference is \sim equal to that for the compact object coming and going. Unfortunate this may have been, but it is of considerable interest, proving to be a direct result of the mass ratio of the binary. If it is indeed correct that the radiating material is spilled from L_2 , the implication is that the speed of the L_2 point is twice the speed of the compact object (175 km s^{-1}) and so its radius is twice the orbit radius. This ratio is a function of the mass ratio q [11]—it is obvious that, for a small value of q , the speeds of the compact object and L_2 would be equal. The observed factor of 2 corresponds to a mass ratio of 0.7. This is the value established, quite independently, for this binary system [1]. The radiating flare environment, conversely, provides a measure of mass ratio q . At this point, it is illuminating to return to Figure 1.

4. Qualitative Analysis of Figure 1

The crude representation of a model based on an accretion disk orbiting the compact object gave the curves in Figure 1. In that model, the red trajectory is contributed by the rim rotating locally away along the line of sight, the blue trajectory from the opposite side. The two oscillate in phase with the orbital motion of the compact object. The red trajectory is augmented by an infalling stream near phase zero, the blue augmented near phase 0.5. The model as illustrated displays idealised trajectories, to represent the data points. To the same level of approximation, we now realise, it could equally well represent the radiating material spilled onto escape orbits through the L_2 point. Such a configuration at any one instant presents a spiral when viewed normal to the orbit of the binary. Viewed in the plane of the orbit, the blue is contributed primarily by material leaving close to the approaching L_2 point, with red receding from earlier ejection. The red is contributed primarily when the L_2 point is receding, at which time, the blue is contributed by earlier source material (now further out and slower). As the spiral rotates, both trajectories oscillate redward and

blueward together, faking the orbital motion of a compact object with an accretion disk. Material from the Companion flowing towards L_2 (or leaving with a significant component of velocity normal to the motion of the L_2 point) is all that is needed to complete the analogy. It is then no surprise that the trajectories in Figure 1 are a good crude representation of the data. These can now be taken as evidence for spiral aspects to the flare ejecta, and, hence, for the mass ratio of the binary.

5. Quantitative Analysis

There are useful numerical results. These are conveniently approached via a simple version of the spiral trail leaving the L_2 region. Take as a model for the spiral a succession of quarter circles, each quarter having a larger radius and linked tangentially to its predecessor. When this spiral is looked at edge on, tangential to the start of the first segment with speed V , that speed is perceived at a radius R , the radius of the first segment about the binary centre of mass. On the opposite side, the radius is greater, and the speed is less; the end of the second segment has speed v at a radius r and is tangential to the line of sight. Conservation of angular momentum requires that these are related by $RV = rv$. We do not know the radius at which ejecta light up and so take for R the radius of the L_2 point, $\sim 1.2A$, where A is the separation of the two components of the binary. The speed of the L_2 point is a little under 400 km s^{-1} , but we do not know the velocity vectors of ejecta leaving L_2 . The first half cycle in Figure 1 suggests that V is rather more than 500 km s^{-1} and $V - v \sim 350 \text{ km s}^{-1}$.

V is unlikely to be much more than 500 km s^{-1} . With these numbers, we solve to obtain the quantities v, r characteristic of the second segment of the spiral. The results are then $r \sim 4A$, $v \sim 150 \text{ km s}^{-1}$; in half a period, the radius has increased by $\sim 3A$. This is a mean rate of increase of $\sim 295 \text{ km s}^{-1}$ between the start of the first segment and the end of the second. If velocity V were as great as 600 km s^{-1} , then $r \sim 3A$, $v \sim 250 \text{ km s}^{-1}$, and the radial speed $\sim 200 \text{ km s}^{-1}$. For comparison, material leaving the L_2 point tangentially with the local escape velocity follows a parabolic trajectory. About 8 days later, it is moving opposite to the L_2 motion, at a radius of $3.4A$ and a speed of $\sim 180 \text{ km s}^{-1}$ [11]. Constructing the spiral from successive quarter circles should be an adequate approximation and might be used as a basis for modelling the observations in [10].

6. Relation to Other Calculations

These numbers are reasonable. Fabrika [12] first discussed the spiral structure resulting from overflow from the L_2 point, with an outgoing component $\sim 200 \text{ km s}^{-1}$; when the jets are more or less in the plane of the sky, there are absorption features with about this speed. Fabrika also estimated an “orbital step” in the spiral of about $4A$ [12]. The GRAVITY data [10] show rotational motion $\sim 500 \text{ km s}^{-1}$ at a radius $\sim A$ (Figure 3 of [10]) and were interpreted by the authors as centrifugal expulsion of the circumbinary disk, with a radial component of $\sim 230 \text{ km s}^{-1}$.

That model has circular symmetry and does not associate the outflow with the vicinity of the L_2 point. Consequently, it lacks the spiral structure of the ejecta characteristic of Fabrika’s proposal and now revealed in the data shown in Figure 1. I have found nothing in the GRAVITY paper [10] that conflicts with such a spiral structure.

7. Conclusions

The flaring in the SS 433 system, as studied in both $H\alpha$ and $\text{Br}\gamma$, is dominated by ejections from the vicinity of the L_2 point. The spiral structure of the ejecta predicted in [12] has now been confirmed observationally for the first time. The remarkable resemblance of the flare spectral shapes to those expected from an accretion disk is now understood and may be taken as providing a measure of the mass ratio. The source of the ejected material must be eruptions of the Companion, feeding in addition accretion by the compact object and the wind from the accretion disk. Overflowing the outer Roche lobe, the ejecta light up to contribute the red and blue extremes of the flaring $H\alpha$ line shapes. One might venture to

speculate that the ejected material does not merely dribble out through the L_2 point, but is actively discharged. The wind from the accretion disk doubles in speed [7] (but the shape of the optical continuum from the photosphere does not change [9]), and both the wind and the spreading spiral become part of the local environment of the microquasar SS 433.

Funding: This research received no external funding.

Data Availability Statement: No new data were created.

Conflicts of Interest: The author declares no conflict of interest.

References

1. Bowler, M.G. SS 433: Two robust determinations fix the mass ratio. *Astron. Astrophys.* **2018**, *619*, L4. [[CrossRef](#)]
2. Bowler, M.G. SS 433: C II emission from the disk photosphere. *arXiv* **2020**, arXiv:2009.00589.
3. HESS Collaboration; Aharonian, F.; Benkhali, F.A.; Aschersleben, J.; Ashkar, H.; Backes, M.; Martins, V.B.; Batzofin, R.; Becherini, Y.; Berge, D.; et al. Acceleration and transport of relativistic electrons in the jets of the microquasar SS 433. *Science* **2024**, *383*, 402–406. [[PubMed](#)]
4. Bowler, M.G.; Keppens, R. W50 and SS 433. *Astron. Astrophys.* **2018**, *617*, A29. [[CrossRef](#)]
5. Bowler, M.G. W50 morphology and the dynamics of SS 433 formation. *arXiv* **2024**, arXiv:2008.10042v2.
6. Schmidtbreick, L.; Blundell, K.M. The emission distribution in SS433. *Proceeding Sci. (MQW6)* **2006**, *94*, 1–6.
7. Blundell, K.M.; Schmidtbreick, L.; Trushkin, S. SS433's accretion disc, wind and jets: Before, during and after a major flare. *Mon. Not. R. Astron. Soc.* **2011**, *417*, 2401–2410. [[CrossRef](#)]
8. Bowler, M.G. SS 433: The accretion disk revealed in H α . *Astron. Astrophys* **2010**, *516*, A24. [[CrossRef](#)]
9. Bowler, M.G. SS 433 Optical Flares: A New Analysis Reveals Their Origin L_2 Overflow Episodes. *Galaxies* **2021**, *9*, 46. [[CrossRef](#)]
10. Waisberg, I.; Dexter, J.; Petrucci, P.O.; Dubus, G.; Perraut, K. Super-Keplerian equatorial outflows in SS 433. *Astron. Astrophys* **2019**, *623*, A47. [[CrossRef](#)]
11. Bowler, M.G. Interpretation of observations of the circumbinary disk of SS 433. *Astron. Astrophys* **2010**, *521*, A81. [[CrossRef](#)]
12. Fabrika, S.N. An extended disc around SS 433. *Mon. Not. R. Astron. Soc.* **1993**, *261*, 241–245. [[CrossRef](#)]

Disclaimer/Publisher's Note: The statements, opinions and data contained in all publications are solely those of the individual author(s) and contributor(s) and not of MDPI and/or the editor(s). MDPI and/or the editor(s) disclaim responsibility for any injury to people or property resulting from any ideas, methods, instructions or products referred to in the content.